Tucholke, B.E., Sibuet, J.-C., and Klaus, A. (Eds.)
Proceedings of the Ocean Drilling Program, Scientific Results Volume 210

3. Paleoflow Directions of Albian Basin-Floor Turbidity Currents in the Newfoundland Basin[1]

Richard N. Hiscott[2]

ABSTRACT

Albian turbidites and intercalated shales were cored from ~1145 to 1700 meters below seafloor at Site 1276 in the Newfoundland Basin. Strata at this level dip ~2.5° seaward (toward an azimuth of ~130°) based on seismic profiles. In contrast, beds dip an average of ~10° in the cores. This higher apparent dip is the sum of the ~2.5° seaward dip and a measured hole deviation of 7.43°, which must be essentially in the same seaward direction. Using the maximum dip direction in the cores as a reference direction, paleocurrents were measured from 11 current-ripple foresets and 11 vector means of grain fabric in planar-laminated sandstones. Five of the planar-laminated sandstone samples have a grain imbrication ≥8°, permitting specification of a unique flow direction rather than just the line-of-motion of the current. Both ripples and grain fabric point to unconfined flow toward the north-northeast. There is considerable spread in the data so that some paleoflow indicators point toward the northwest, whereas others point southeast. Nevertheless, the overall pattern of paleoflow suggests a source for the turbidity currents on the southeastern Grand Banks, likely from the long-emergent Avalon Uplift in that area. On average, turbidity currents apparently flowed axially in the young Albian rift, toward the north. This is opposite to what might be expected for a northward-propagating rift and a young ocean opening in a zipperlike fashion from south to north.

[1]Hiscott, R.N., 2007. Paleoflow directions of Albian basin-floor turbidity currents in the Newfoundland Basin. *In* Tucholke, B.E., Sibuet, J.-C., and Klaus, A. (Eds.), *Proc. ODP, Sci. Results,* 210: College Station, TX (Ocean Drilling Program), 1–27. doi:10.2973/odp.proc.sr.210.103.2007
[2]Earth Sciences Department, Memorial University of Newfoundland, St. John's NF, A1B 3X5, Canada.
rhiscott@mun.ca

Initial receipt: 5 January 2006
Acceptance: 14 July 2006
Web publication: 14 May 2007
Ms 210SR-103

INTRODUCTION

The source of deep-sea turbidites can be inferred from major-component petrography (e.g., Dickinson et al., 1983; Zuffa, 1985; **Marsaglia,** this volume), heavy minerals (Hubert, 1971), trace element or rare earth element geochemistry (e.g., McLennan et al., 1990), and/or paleocurrent analysis (Potter and Pettijohn, 1963). The latter technique might not point unambiguously to the source region if flows took a circuitous path to the site of deposition (e.g., Zuffa et al., 2000). This paper employs paleocurrent analysis using flow directions determined from ripple foresets and grain-fabric studies of Albian sandstone turbidites recovered in Hole 1276A east of the Grand Banks of Newfoundland (Fig. **F1**). No downhole geophysical logs were obtained in Hole 1276A, preventing the reorientation of core samples to a modern geographic reference frame using, for example, high-resolution Formation MicroScanner (FMS) images. In the absence of this type of straightforward way to reorient samples, a different approach was used: seismic dips, bedding dips in cores, and the availability of a single measurement of the amount of the borehole deviation (but not its direction) were all considered in order to infer the azimuth of the dip line in core pieces. The dip line was then used as a reference direction to reorient the core samples and paleocurrent measurements.

Site 1276 is located in 4560 m of water east of the Grand Banks and south of Flemish Cap. Coring began 800 meters below seafloor (mbsf) and proceeded to approximately the Aptian/Albian boundary at 1739 mbsf. The sedimentation rate was generally <5–7 m/m.y. from the earliest Oligocene to the Cenomanian but was ~20–100 m/m.y. during the Albian. As a consequence, the Albian section predominates and extends from ~1145 to 1700 mbsf (Fig. **F2**). This interval consists of ~⅔ hemipelagic bioturbated mudrocks, ~⅓ mud-dominated gravity-flow deposits, and volumetrically minor but numerous black shales rich in terrestrial organic carbon. The Albian succession belongs to previously defined lithologic Subunits 5B and 5C (Shipboard Scientific Party, 2004a). The proportion of black shales decreases below ~1400 mbsf, whereas the proportion of thick bedded to very thick bedded muddy turbidites, some as graded units thicker than 2 m, increases below ~1500 mbsf (Fig. **F3**). The thicker turbidites are characterized by ductile soft-sediment deformation and pseudonodule development. Sorting in these beds is poor, and there are common plant fragments and mud clasts.

The Albian succession corresponds to seismic Sequence B (Shipboard Scientific Party, 2004a), which is characterized by mostly parallel reflectors that typically extend for tens to hundreds of kilometers. In its upper part, minor local downlap and onlap suggest some depositional relief. There is a slight seaward dip over a broad area around Site 1276. This dip is crucial to unraveling paleocurrents in the Albian succession and will be discussed more fully in **"Data and Methods,"** p. 4.

During the Albian, a narrow seaway had opened between the Grand Banks and the western margin of Iberia (Fig. **F4**). The central segment of the North Atlantic Ocean was much wider; northwest Africa had separated from Nova Scotia in the Middle Jurassic. By the Albian, the African plate had slid along the south Newfoundland transform margin to a position well east of the Grand Banks. Hence, the narrow seaway at Site 1276 faced a wide ocean basin to the south. Potential source areas for the Albian turbidites include Flemish Cap, the southern Grand Banks, and the more northerly extension of the propagating North At-

F1. Location of ODP Site 1276, p. 15.

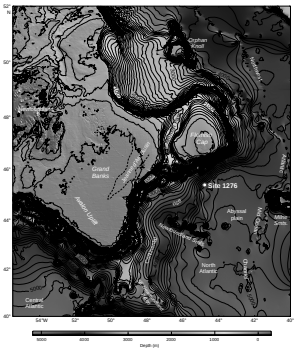

F2. Hole 1276A lithologic column correlated to time-equivalent stratigraphy, p. 16.

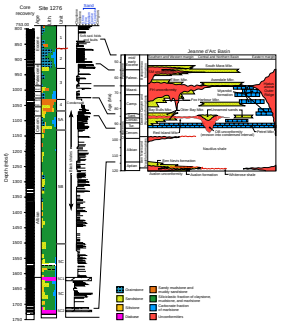

F3. Graphic section of Cores 210-1276A-89R to 93R, p. 17.

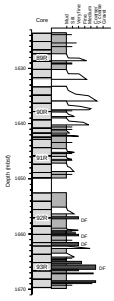

F4. Reconstructions of the Cretaceous North Atlantic region, p. 18.

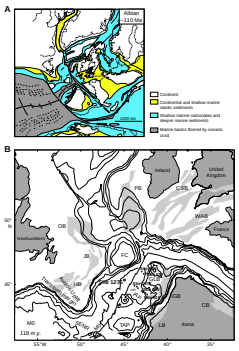

lantic rift system. The nascent mid-ocean ridge to the east of Site 1276 likely prevented bottom-hugging gravity currents from reaching the area from the Iberian margin, but this scenario cannot be ruled out a priori.

The time-equivalent succession in the Jeanne d'Arc Basin of the Grand Banks consists of the lowest Albian "O35 Upper Sandstone" of the Ben Nevis Formation, and the Nautilus Shale (Ainsworth et al., 2005) (Fig. F2). Detritus in the Ben Nevis Formation was derived from the southwest and south (Ainsworth et al., 2005). The Nautilus Shale accumulated in a well-oxygenated open-shelf environment, which developed during a period of transgression.

Paleoflow in a turbidite succession can be determined by measurement of the orientation of sedimentary structures: sole markings, foresets of current-ripple cross-lamination, and foresets of dune-scale cross-bedding. In small diameter cores, sole markings (e.g., flutes, grooves) are rarely encountered and are therefore not a viable structure for routine analysis. Dune-scale cross-bedding is extremely rare in turbidites, whereas the migration direction of current ripples in the T_c division (c division of Bouma, 1962) can commonly be measured, even in cores.

An alternative to the use of sedimentary structures is the microscopic measurement of the grain fabric of sandstones. Numerous studies have shown that sand grain orientation is a reliable indicator of paleoflow direction in sandy turbidites (McBride and Kimberly, 1963; Spotts, 1964; Colburn, 1968; Onions and Middleton, 1968; Parkash and Middleton, 1970; Hiscott and Middleton, 1980). The long axes of the detrital particles are preferentially oriented parallel with the paleoflow direction (Johansson, 1976; Allen, 1984, p. I-219). Even very large elongate fossils, for example graptolite stipes in Paleozoic deposits, are aligned with the paleocurrent (Enos, 1969; Parkash and Middleton, 1970), although they tend to lie in bedding and therefore do not show imbrication. In contrast, the average sand-sized elongate particles in planar-laminated or stratified sandstone turbidites tend to be inclined into the current, producing an imbrication of ~10°–30° (Hiscott and Middleton, 1980), although lower values of imbrication are not uncommon (Allen, 1984, p. I-219).

The alignment of detrital grains can be measured directly using microscopic techniques or indirectly using anisotropy of magnetic susceptibility (AMS). AMS measures the preferred orientation of magnetic grains in a sandstone or siltstone (Rees, 1965; Taira, 1976; Hiscott et al., 1997). Like any other paleocurrent indicator, grain fabric is a measure of the local flow vector and not the average flow field. Parkash and Middleton (1970) showed that velocity vectors in turbidity currents meander in a streamwise direction, so that paleoflow indicators in a single bed can vary by tens of degrees either downcurrent or stratigraphically upward in the deposit of a single gravity flow (see also Onions and Middleton, 1968; Hiscott and Middleton, 1980). The implication is that a number of measurements of paleoflow must be averaged in order to assess the ancient dispersal direction.

DATA AND METHODS

Establishing the Original Orientation of Core Pieces and Samples

Paleocurrent measurements must be placed within a geographic coordinate system. At first, the correct reorientation of core pieces and grain-fabric samples analyzed from Hole 1276A seemed an impossibility because of the lack of borehole images or other guides to core orientation. However, three observations prompted the author to look for an alternative way to orient core samples:

1. Apparent dip measurements from crossing multichannel seismic reflection lines (Fig. **F5;** Table **T1**) indicate that the reflections in Subunits 5B and 5C, below a depth of ~1250 mbsf, dip toward ~130° (seaward) at an average angle of ~2.5°.
2. The Tensor tool was deployed deep in Hole 1276A and indicated that the borehole is deviated 7.43° from the vertical at a depth of 1652 mbsf.
3. Maximum dips measured in X-ray computed tomography (CT) scans of long sections of unbroken core are as much as ~15° and average ~10° (Fig. **F6** and supporting discussion in **"Establishing the Amount of Maximum Apparent Dip from CT Images,"** p. 5).

It is well known that holes bored into dipping strata tend to naturally deviate either updip or downdip (McCray and Cole, 1959). The only way that bedding can dip an average of 10° relative to the borehole, when the true dip is ~2.5°, is if the borehole had deviated downdip. This would result in an apparent dip in cores which is the sum of the true dip and the borehole deviation. In the case of Hole 1276A, the deviation direction must be almost exactly downdip (i.e., toward ~130°) to account for the observed average apparent dip measured from the CT scans (Fig. **F6**). The fact that both the true dip and the hole deviation are toward ~130° means that the dip line in any piece of core can be assumed to point toward this same azimuth. This result provides a critical reference direction for the paleocurrent measurements reported in this paper.

Depth-converted multichannel seismic reflection profiles were provided to the author by shipboard participant D. Shillington (extracted from profiles in Shillington et al., 2006). Line 2 crosses Site 1276 in the dip direction (N125E), and Line 303 crosses the site in the strike direction (N35E). Six prominent dipping reflections were selected in the depth range corresponding to the Albian succession. Apparent dips were measured in both the dip and strike profiles, and the Macintosh application Stereonet (version 6.3X) was used to determine the true dip directions and amounts after accounting for the vertical exaggeration in the profiles (Table **T1**). The data were then averaged to give the true dip of the Albian succession. One of the apparent dips in the strike profile (Line 303) is 1.44° toward the northeast; this is different from the other five apparent dips both in direction and amount (Fig. **F5**). However, the other five apparent dips on this profile are all significantly smaller than the corresponding apparent dips in the dip profile (Line 2), indicating that the structural dip line must be quasi-parallel to the orientation of Line 2. Omitting the seemingly anomalous northeasterly

F5. Depth-converted seismic reflection profiles through Site 1276, p. 19.

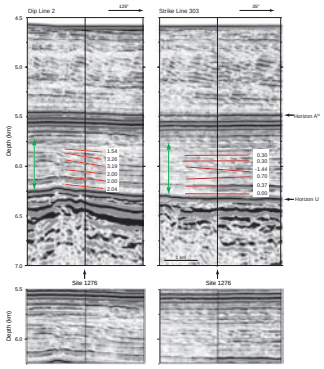

T1. Apparent dips and calculated true dips of six reflections, p. 24.

F6. Average core-by-core maximum dip, p. 20.

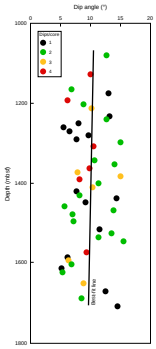

apparent dip of 1.44° would change the orientation of the calculated average dip line by <6°, from 128.6° to 134.2°.

Establishing the Amount of Maximum Apparent Dip from CT Images

An X-ray CT scanner was used for routine prescreening of unsplit whole cores. The unit was manufactured by Lawrence Berkeley National Laboratory (Berkeley Lab) and is described in detail by Freifeld et al. (2003). During scanning, the core was rotated around its vertical axis 180 times in steps of 2° until a complete rotation of 360° was achieved. The gantry holding the X-ray source and detector was raised and lowered by a belt-driven actuator to permit the examination of selected 15-cm-long regions of the core. The X-ray source has a tungsten target and a 250-µm beryllium window, delivering up to 130 kV at 65 W. It has a variable focal-spot size that increases from 5 µm at 4 W to 100 µm at 65 W. An image intensifier with a cesium iodide phosphor input screen was coupled to a digital camera for image capture (a Sony XC-75 with a resolution of 768 × 494 pixels and a signal-to-noise ratio of 56 dB). Ten frames of the same image were acquired and averaged to reduce camera noise. Each of the 180 images acquired at each position records the integrated densities across the entire thickness of the core.

On shore, the archived CT scans were viewed using the special-purpose program XVIEW developed by W.G. Mills of the Ocean Drilling Program (ODP)/Integrated Ocean Drilling Program. Images were selected from long intervals of unbroken or slightly fractured core in which dipping beds were clearly visible. Up to four good-quality images fitting these criteria were studied in individual 9.6-m-long cores. XVIEW allows sequential examination of the 180 images generated by rotation of the gantry during acquisition of the images. This was done until the maximum dip angle (i.e., the "maximum apparent dip") was displayed. This is not, of course, the true dip of the strata because it is the sum of the borehole deviation and some component of the bedding dip. Using a cursor-controlled tool in XVIEW, this maximum dip angle was precisely measured. For each 9.6-m-long core, all measured maximum dip angles were averaged in order to minimize the effects of slight tilting of pieces of core in the plastic liners.

Ripple and Grain-Fabric Paleocurrent Measurements

During Leg 210, the author measured paleoflow direction from 11 sets of cross-lamination forming the T_c divisions of turbidites (Table T2). These were measured in degrees clockwise or counterclockwise from the maximum dip in the particular piece of core. Such measurements are believed to be accurate to ±10° because of uncertainties in determination of the dip direction of local bedding and the maximum dip direction of ripple foresets.

T2. Ripple migration directions recorded in core pieces, p. 25.

Sixteen sandstone samples were taken from the planar-laminated T_b divisions of turbidites (b divisions of Bouma, 1962), but only where the dip direction of the laminae could be easily determined from the sample itself. For each sample, a thin section was cut parallel to the laminae, and the maximum dip direction was marked on the microscope slide. All thin sections were cut so that the view, downward through the slide, is stratigraphically downward.

The orientation of 200 or more grains was measured in each bedding-parallel thin section, following procedures described by Hiscott and Middleton (1980). In some samples, the elongate grains are mostly silicate minerals like quartz and feldspar, but in many finer-grained sandstones, the elongate clasts are predominantly plant fragments. Because of the small sample size and dearth of larger elongate silicate grains in some samples, all particles with a clear orientation were selected for measurement. The outline of each elongate grain larger than ~0.1 mm and with a b/a axis ratio >1.5 was traced onto a large sheet of stiff clear plastic laid on the 50-cm-diameter viewing window of a Baty Shadowmaster (model SM20B) microprojector, at a magnification of 100×. After all grains in a particular view were traced, the thin section was mechanically advanced to a new position. This process continued until 200 grains were traced. The dip line was transferred to the plastic sheet and orientations to the nearest degree of the long axes of the 200 grains were measured relative to the dip line, in the range of 0°–179° (i.e., the smallest possible angle was recorded). Symmetrical equal-area rose diagrams were plotted for each sample after grouping the data into 10° classes. Equal-area plots are preferred because the human eye attaches more weight to the area of a slice in a pie-type diagram than to its length (Nemec, 1988; Baas, 2000).

The vector mean (υ) and vector magnitude (L) were calculated for each sample using procedures outlined by Harrison (1957). The Tukey χ^2 test (Middleton, 1965) was used to determine the significance of each orientation. Only those samples with a significance level (SL) ≤ 0.10 were deemed to have a preferred orientation and were selected for analysis of imbrication direction. By convention, the vector mean is recorded as the smallest possible angle so is assigned an azimuth of 000°–179° rather than 000°–359°.

For a sample size of 200 and a vector magnitude corresponding to a SL ≤ 0.10, the 90% confidence interval about the mean is bounded by approximately $\upsilon - 5°$ and $\upsilon + 5°$ (fig. 3 in Curray, 1956). The true vector mean will lie outside these limits one time in ten. To this uncertainty must be added realistic errors associated with determining the dip direction in each piece of core. To account for these uncertainties, it is proposed that orientation measurements be considered accurate to no better than ±15°. This does not include any uncertainty associated with establishing the geographic reference direction of 130°.

For each sample with SL ≤ 0.10, the remainder of the rock sample was cut perpendicular to its planar lamination and parallel to the paleoflow direction deduced from grain alignment in the first thin section. In these bedding-perpendicular thin sections, the orientation of 200 grains was measured as described above, but with the lamination itself as the reference line. Equal-area rose diagrams provide a visual summary of the data. The discovery of a significant imbrication allows the unambiguous selection of υ or $\upsilon + 180°$ as the true paleoflow direction.

The vector magnitude (i.e., strength) of the grain fabric tends to be considerably stronger perpendicular to layering than parallel to layering (Harrison, 1957). Such high vector magnitudes result in more closely spaced 90% confidence limits bounded by approximately $\upsilon - 3°$ and $\upsilon + 3°$. The actual vector mean of the imbrication will be outside these limits one time in ten and will be less than the lower confidence limit (i.e., closer to the horizontal) only one time in twenty. However, there are additional errors and uncertainties in picking the plane of the lamination and measuring individual grains, including operator variation (Hiscott and Middleton, 1980); these likely contribute to about ±5°

additional error. To account for these uncertainties, it was decided to only consider imbrications as being significant if 8° or greater.

Many Hole 1276A samples have strong grain alignment in sections cut perpendicular to bedding, but this alignment cannot be used to uniquely specify the paleoflow direction (rather than the line-of-motion of the current) unless the average long axis of the grains is inclined ≥8° to the sedimentary layering. Not surprisingly, samples with plant fragments as a majority of the measured fabric elements tend not to show a sufficiently high imbrication angle to permit a decision on the paleoflow direction (i.e., to choose between υ and υ + 180°). These fragments are larger and less dense than associated silicate particles and, like the graptolite stipes in some Paleozoic sandstones, tend to lie horizontally in the lamination.

RESULTS

If the average dip angle in the cores (Fig. F6) had been less than ~10°, then there would have been two directions in which Hole 1276A might have been deviated, both of which would have satisfied the requirement that the deviation angle plus the actual apparent dip measured from the horizontal must equal the dip seen in the cores. These two directions would have been disposed to either side of the true dip direction of the Albian strata. The fact that the average dip angle measured relative to the nominal vertical axes of the cores is ~10° greatly simplifies the paleocurrent analysis because the only logical solution is that the hole is deviated in the direction of the true dip.

Because borehole images and standard geophysical logs were not obtained in Hole 1276A, confirmation that the dip line (from seismic reflection profiles) provides a reliable geographic reference frame for the fabric samples (with their internal dipping laminae) is difficult to establish. Paleomagnetic data might provide an independent method for reorienting core pieces, if a magnetic-field orientation of known age can be extracted from the cores. By chance rather than planning, two fabric samples (Samples 210-1276A-67R-5, 120–122 cm, and 84R-1, 111–113 cm) were taken in the same pieces of split core as two paleomagnetic samples (Samples 210-176A-67R-5, 101–103 cm, and 84R-1, 100–102 cm); no other fabric samples are similarly co-located with paleomagnetic samples. Zhao (this volume) determined declination/inclination pairs of 044.5°/–70.3° and 342.8°/+73° on the paleomagnetic samples from Sections 210-1276A-67R-5 and 84R-1, respectively. X. Zhao (pers. comm., 2005) believes that the inclinations in these samples are sufficiently close to the expected earliest Albian (~112 Ma) inclination at Site 1276 (i.e., 59° ± 6.7°) to use the measured declinations in these samples to reorient the core pieces independent of the dip-line method. The early Albian declination at Site 1276 was 341.7° (based on a North American 110-Ma reference pole at 75.4°N, 208.8°E, and the location of Site 1276 at 45.4°N, 44.6°W).

Relative to the conventions used by ODP paleomagnetists to specify orientations of archive and working halves (Shipboard Scientific Party, 2004b), the rotations needed to correctly reorient the co-located paleomagnetic and fabric samples in Section 210-1276A-67R-5 are 243° counterclockwise (paleomagnetic method; X. Zhao, pers. comm., 2005) and 320° counterclockwise (dip-line method). Errors for each calculated rotation are estimated to be approximately ±10°–15°. For the co-located

samples in Section 210-1276A-84R-1, the equivalent paleomagnetic and dip-line rotations are 000° and 040° counterclockwise, respectively.

The attempt to cross-check paleomagnetic and dip-line methods for reorienting core pieces at Site 1276 is deemed to have been unsuccessful. Using maximum error estimates, the discrepancies between the methods are ~50° and 10° (Sections 210-1276A-67R-5 and 84R-1, respectively). X. Zhao (pers. comm., 2005) has indicated to the author that it is a big assumption that his two samples retain the declination and inclination of the earliest Albian magnetic field. If they do not, then the apparent discrepancies carry no weight. Even the assessment that the inclinations in the paleomagnetic samples are close to the earliest Albian inclination might be erroneous because the paleomagnetic measurements took no account of the ~10° dip of bedding in the cores. Clearly, validation of (1) the 130° reference direction used in this paper to reorient the paleoflow determinations and (2) the method of referencing paleocurrent data to the dip line in individual samples awaits an unambiguous, independent method of core reorientation. It is believed that logging of Hole 1276A, including acquisition of FMS images, would be required.

Using the dip-line method for reorientation, ripple migration directions range from north-northwest to southeast (azimuths of 340° to 130°; Table **T2**). The average of these measurements is toward the northeast (060°). Equal-area rose diagrams of 11 fabric samples with SL ≤ 0.10 show a range of paleoflow directions (Fig. **F7;** Table **T3**). Only five of these samples possess an imbrication of ≥8° (Fig. **F8;** Table **T4**). Four of these support the north-northeasterly direction determined from ripple foresets (Fig. **F9A**), whereas the fifth is anomalous in suggesting paleoflow toward the west-northwest (289°). This last sample had a marginal imbrication of 8° with a relatively low vector magnitude, so the true flow direction for this sample might be toward the east-southeast instead.

DISCUSSION

Even if an error of ±30° is assigned to the determination of the geographic reference direction, the mean paleoflow direction remains in the northeast quadrant. A global counterclockwise rotation of the reference direction by 30° results in many of the paleocurrents pointing up the continental slope toward the Grand Banks. This is believed to be an unrealistic scenario, particularly because the young mid-ocean ridge just to the east would have been a barrier to gravity-flow transport from Iberia. Therefore, only two cases will be discussed: that the reference direction is indeed 130° (Fig. **F9A**) or that the true reference direction (and local dip direction) is closer to 160° (Fig. **F9B**).

A 130° reference direction implies paleoflow toward the north-northeast (Fig. **F9A**) and implicates the Avalon Uplift as the likely source area. The Avalon Uplift became a positive tectonic element in the Late Jurassic (DeSilva, 2004) and remained an important source for sandstones in the nearby Jeanne d'Arc Basin throughout the Early Cretaceous, undoubtedly shedding sediment into the nascent Newfoundland Basin at that time. It has been postulated that the Avalon Uplift is, in part, a response to strike-slip motions along a fault trace extending from the southern Grand Banks into mainland Nova Scotia (Pe-Piper and Piper, 2004). Lower Cretaceous sandstones in the Jeanne d'Arc Basin commonly contain terrestrial plant debris, but this similarity with

F7. Equal-area rose diagrams summarizing bed-parallel grain fabric, p. 21.

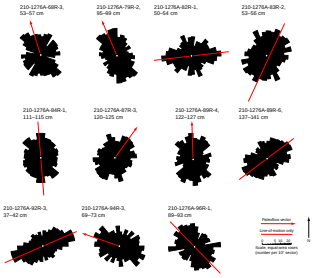

T3. Summary statistics for bed-parallel thin sections, p. 26.

F8. Equal-area rose diagrams summarizing bed-perpendicular grain fabric, p. 22.

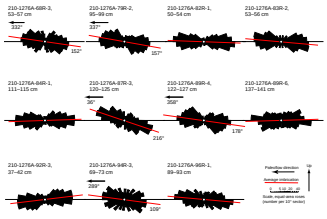

T4. Summary statistics for bed-perpendicular thin sections, p. 27.

F9. Unit vector plots of 11 ripple foreset dips and vector means for 11 grain-fabric determinations, p. 23.

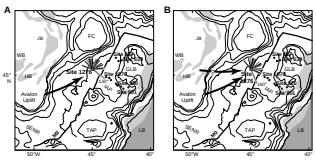

the Site 1276 Albian sandstones does not require a common source. In the Figure F9A scenario, Flemish Cap and areas farther north provided no detritus. This might have been because they were largely submerged during the high sea levels of the Albian, or because of relief created by fracture zones oriented orthogonal to the continental margin that would have compartmentalized the sediment dispersal and prevented the input of detritus from farther north.

Dispersal of the Albian turbidity currents from the Avalon Uplift and environs would require a strong component of northward axial transport into the opening rift arm between the Grand Banks and Iberia. Axial transport is quite common in ancient elongate basins, with the premier examples being provided by foreland basins at convergent margins (e.g., Enos, 1969). The young Newfoundland Basin would have been less constricted than a foreland basin, so that gravity currents would have been more free to deviate to the left or right of the average flow direction, perhaps accounting in part for the considerable scatter of paleocurrent measurements. As noted earlier, paleoflow indicators in Ordovician turbidites have been shown to swing from side to side from the base to the top of those deposits. Such free meandering of local flow vectors would be facilitated by transport across a relatively flat basin floor (Fig. F5). The presence of thick to very thick turbidites with thick muddy caps in the Albian succession at Site 1276 (Fig. F3) is typical of basin-plain settings (Pickering et al., 1989) and supports the notion of a relatively flat featureless area where successive currents could take somewhat different routes across the basin floor.

A 160° reference direction implies paleoflow toward the east (Fig. F9B) and permits detrital supply from a broader source area across the southern Grand Banks. Turbidity currents could have taken a path directly downslope, essentially orthogonal to the young continental margin. However, much of this part of the Grand Banks is occupied by Cretaceous basins which themselves contain Albian marine shales (e.g., Nautilus Shale of Jeanne d'Arc Basin). These submerged or low-lying areas are unlikely sources for the thick, terrigenous Albian succession in the Newfoundland Basin.

There are no strong criteria to guide the selection of Figure F9A or F9B as the more realistic reconstruction of Albian paleoflow. However, either option implicates the Avalon Uplift as a primary source for the large volumes of Albian sediment present in the Newfoundland Basin. The southeasternmost part of this long-lived high is underlain by rocks of the Meguma Zone of the Canadian Appalachians (Haworth and Lefort, 1979; Schenk, 1995). Where exposed in Nova Scotia, the Meguma Zone is largely underlain by Lower Paleozoic shales/slates and sandstone turbidites of the Goldenville and Halifax groups (Schenk, 1995). The rest of the Grand Banks is underlain by Precambrian–Lower Paleozoic rocks of the Avalon Zone (Williams et al., 1995), covered in large part by younger Carboniferous rocks (Sanford et al., 1979) believed to be mostly continental to deltaic sandstones and shales similar to the outcropping Carboniferous strata in the Canadian Appalachians. All of these rock types would be suitable sources for the Albian succession recovered at Site 1276. During the Early Cretaceous, this area had a latitude of ~30°N (Irving, 1979; Dercourt et al., 1986) and a maritime climate. These conditions would have promoted chemical weathering, fluvial transport of erosional products to the coast, and subsequent remobilization into the deep Newfoundland Basin by turbidity currents. A fairly direct fluvial–deltaic supply is indicated by the abundance of

terrestrial organic material in the Albian succession (Shipboard Scientific Party, 2004a) and the textural immaturity of the sediments.

The North Atlantic rift opened progressively from the southern Grand Banks toward the north. With this zipperlike opening, it might be predicted that the region around the propagating rift tip would be the most highly elevated area and therefore the most likely source for coarser-grained detritus. An ancient example showing this polarity is the Athapuscow Aulacogen (Hoffman, 1969), which is the failed arm of a rift system in the Proterozoic of the Great Slave Lake area, northern Canada. In that system, siliciclastic sediments of the Sosan Group were transported axially from the inland tip of the failed rift toward the triple junction. If the North Atlantic rift had behaved in the same way, then one might have expected southward axial flow between the Grand Banks and Iberia from source areas to the north. However, there was already an Albian seaway extending well to the north of the Grand Banks (Dercourt et al., 1986; Ziegler, 1988; Gradstein et al., 1990), with marine sediments widely distributed in basins of the United Kingdom shelf and into the Bay of Biscay (Fig. **F4A**). This seaway signifies low relief in the rift zone, which allowed high Albian sea levels to inundate large areas. Detritus from adjacent lands would have been used to fill local accommodation space, rather than being shunted farther south. As noted above, fracture zones oriented transverse to the rift zone also might have played a role in preventing sediment supply to Site 1276 from the north (cf. Escanaba Trough in the modern eastern Pacific, Zuffa et al., 2000).

Without significant detrital input from the northern extremities of the propagating rift, the persistent Avalon Uplift took on this role and effectively reversed the expected polarity of paleoflow in the Newfoundland Basin by shedding large amounts of detritus onto the western slopes of the narrow Albian ocean basin. From this marginal position, a variety of slope failures generated large-volume mud-laden turbidity currents that formed the typical basin-plain succession seen at Site 1276.

SUMMARY

1. Cores from Hole 1276A are difficult to orient because of a lack of downhole imagery (e.g., FMS microresistivity images). A provisional reference frame has been developed using the maximum dip direction in cores, which is argued to point down the modern dip toward an azimuth of ~130°.
2. Within the reference frame provided by dip-line measurements, current-ripple foresets in 11 separate turbidites indicate northeastward paleoflow, with considerable scatter in the data. This scatter is attributed to unconfined flow on a basin plain and meandering of the local flow vector in turbidity currents.
3. Eleven of 16 planar-laminated sandstone samples have a well-developed grain fabric, with the average long axis of sand grains parallel to paleoflow. Five of these 11 have a well-developed imbrication which allows specification of a unique flow direction. With one exception, the paleoflow determined from sand-grain fabric is consistent with the north-northeast paleoflow determined from current ripples.
4. Two models are evaluated, one with the 130° dip line and one with a 160° dip line, to consider the maximum level of uncer-

tainty which might exist in the specification of geographic orientations. This uncertainty includes possible errors in determination of the seismic dip direction, the bedding dip in core samples, and the direction of borehole deviation. Both models suggest derivation of the Albian turbidites from the adjacent Grand Banks, specifically from the southeast corner of that platform in the vicinity of the Avalon Uplift. There is no support for a source to the east in Iberia, nor for a source farther north in the developing North Atlantic rift.

5. Although some uncertainty will continue to surround the reorientation of samples and cores used for this study, it has been possible to demonstrate that sand-grain fabric can be used to determine the paleoflow of the Albian turbidites in the Newfoundland Basin. If this area is revisited and borehole images permit a better orientation of Leg 210 or other core samples, then there is clear promise in reevaluating the data in this paper or in applying the same methods to new samples.

ACKNOWLEDGMENTS

I thank the crew of the *JOIDES Resolution* for skillful operations in the Newfoundland Basin. This research used samples and/or data provided by the Ocean Drilling Program (ODP). ODP is sponsored by the U.S. National Science Foundation (NSF) and participating countries under the management of Joint Oceanographic Institutions (JOI), Inc. This study was supported by Natural Sciences and Engineering Research Council of Canada. Travel funding to join the leg was provided by the Dean of Science at Memorial University of Newfoundland (MUN). William (Bill) Mills is thanked for prodigious efforts to ensure operation of the CT scanner at sea, and for writing the XVIEW software. Helen Gillespie was very helpful in overseeing sample preparation for the fabric work at MUN. The SCREECH seismic reflection data (Fig. **F5**) were acquired with support from NSF grant OCE98-19053, B.E. Tucholke and W.S. Holbrook, principal investigators. Critical comments by reviewers David J.W. Piper, William R. Normark, and editor Brian E. Tucholke improved the content of the paper.

REFERENCES

Ainsworth, N.R., Riley, L.A., and Sinclair, I.K., 2005. A mid-Cretaceous (upper Barremian–Turonian) lithostratigraphic and biostratigraphic framework for the Hibernia oilfield reservoir sequence, Jeanne d'Arc Basin, Grand Banks of Newfoundland. *In* Hiscott, R.N., and Pulham, A.J. (Eds.), *Petroleum Resources and Reservoirs of the Grand Banks, Eastern Canadian Margin*. Geol. Assoc. Can. Spec. Pap., 43:45–72.

Allen, J.R.L., 1984. *Sedimentary Structures: Their Character and Physical Basis*. Dev. Sedimentol., 30: Amsterdam (Elsevier).

Andeweg, B., 2002. Cenozoic tectonic evolution of the Iberian Peninsula, causes and effects of changing stress fields [Ph.D. thesis]. Vrije Universiteit Amsterdam.

Baas, J.H., 2000. EZ-ROSE: a computer program for equal-area circular histograms and statistical analysis of two-dimensional vectorial data. *Comp. Geosci.,* 26(2):153–166. **doi:10.1016/S0098-3004(99)00072-2**

Bouma, A.H., 1962. *Sedimentology of Some Flysch Deposits: a Graphic Approach to Facies Interpretation*. Amsterdam (Elsevier).

Colburn, I.P., 1968. Grain fabrics in turbidite sandstone beds and their relationship to sole mark trends on the same beds. *J. Sediment. Petrol.,* 38:146–158.

Curray, J.R., 1956. Analysis of two-dimensional orientation data. *J. Geol.,* 64:117–131.

Deptuck, M.E., MacRae, R.A., Shimeld, J.W., Williams, G.L., and Fensome, R.A., 2003. Revised Upper Cretaceous and lower Paleogene lithostratigraphy and depositional history of the Jeanne d'Arc Basin, offshore Newfoundland, Canada. *AAPG Bull.,* 87(9):1459–1483. **doi:10.1306/050203200178**

Dercourt, J., Zonenshain, L.P., Ricou, L.-E., Kazmin, V.G., Le Pichon, X., Knipper, A.L., Grandjacquet, C., Sbortshikov, I.M., Geyssant, J., Lepvrier, C., Pechersky, D.H., Boulin, J., Sibuet, J.-C., Savostin, L.A., Sorokhtin, O., Westphal, M., Bazhenov, M.L., Lauer, J.P., and Biju-Duval, B., 1986. Geological evolution of the Tethys belt from the Atlantic to the Pamirs since the Lias. *Tectonophysics,* 123(1–4):241–315. **doi:10.1016/0040-1951(86)90199-X**

DeSilva, N.R., 2004. Application of petroleum system logic to Jeanne d'Arc Basin offshore Newfoundland. *In* Hiscott, R.N., and Pulham, A.J. (Eds.), *Petroleum Resources and Reservoirs of the Grand Banks, Eastern Canadian Margin*. Geol. Assoc. Can. Spec. Pap., 43:1–10.

Dickinson, W.R., Beard, L.S., Brakenridge, G.R., Erjavec, J.L., Ferguson, R.C., Inman, K.F., Knepp, R.A., Lindberg, F.A., and Ryberg, P.T., 1983. Provenance of North American Phanerozoic sandstones in relation to tectonic setting. *Geol. Soc. Am. Bull.,* 94:222–235.

Enos, P., 1969. Anatomy of a flysch. *J. Sediment. Petrol.,* 39:680–723.

Freifeld, B.M., Kneafsey, T.J., Tomutsa, L., and Pruess, J., 2003. Development of a portable X-ray computed tomographic imaging system for drill-site investigation of recovered core. *Proc. Int. Symp. Soc. Core Anal.,* 581–586.

Gradstein, F.M., Jansa, L.F., Srivastava, S.P., Williamson, M.A., Bonham-Carter, G., and Stam, B., 1990. Aspects of North Atlantic paleo-oceanography. *In* Keen, M.J. and Williams, G.L. (Eds.), *The Geology of North America* (Vol. 2): *Geology of the Continental Margin of Eastern Canada:* Boulder (Geol. Soc. Am.), 351–389.

Harrison, P.W., 1957. New technique for three-dimensional fabric analysis of till and englacial debris containing particles from 3 to 40 millimetres in size. *J. Geol.,* 65:98–105.

Haworth, R.T., and Lefort, J.P., 1979. Geophysical evidence for the extent of the Avalon zone in Atlantic Canada. *Can. J. Earth Sci.,* 16:552–567.

Hiscott, R.N., Hall, F.R., and Pirmez, C., 1997. Turbidity-current overspill from the Amazon Channel: texture of the silt/sand load, paleoflow from anisotropy of magnetic susceptibility and implications for flow processes. *In* Flood, R.D., Piper, D.J.W., Klaus, A., and Peterson, L.C. (Eds.), *Proc. ODP, Sci. Results,* 155: College Station, TX (Ocean Drilling Program), 53–78. **doi:10.2973/odp.proc.sr.155.202.1997**

Hiscott, R.N., and Middleton, G.V., 1980. Fabric of coarse deep-water sandstones, Tourelle formation, Quebec, Canada. *J. Sediment. Petrol.,* 50:703–722.

Hoffman, P.F., 1969. Proterozoic paleocurrents and depositional history of the east arm fold belt, Great Slave Lake, NWT. *Can. J. Earth Sci.,* 6:441–462.

Hubert, J.F., 1971. Analysis of heavy-mineral assemblages. *In* Carver, R.E. (Ed.), *Procedures in Sedimentary Petrology:* New York (Wiley), 453–478.

Irving, E., 1979. Paleopoles and paleolatitudes of North America and speculations about displaced terrains. *Can. J. Earth Sci.,* 16:669–694.

Johansson, C.E., 1976. Structural studies in frictional sediments. *Geogr. Ann., Ser. A,* 4:201–301.

McBride, E.F., and Kimberly, J.E., 1963. Sedimentology of the Smithwick shale (Pennsylvanian), eastern Llano region, Texas. *AAPG Bull.,* 47:1840–1854.

McCray, A.W., and Cole, F.W., 1959. *Oil Well Drilling Technology:* Norman (Univ. Oklahoma Press).

McLennan, S.M., Taylor, S.R., McCulloch, M.T., and Maynard, J.B., 1990. Geochemical and Nd-Sr isotopic composition of deep-sea turbidites: crustal evolution and plate tectonic associations. *Geochim. Cosmochim. Acta,* 54(7):2015–2050. **doi:10.1016/0016-7037(90)90269-Q**

Middleton, G.V., 1965. The Tukey chi-squared test. *J. Geol.,* 73:547–549.

Nemec, W., 1988. The shape of the rose. *Sediment. Geol.,* 59(1–2):149–152. **doi:10.1016/0037-0738(88)90105-4**

Onions, D., and Middleton, G.V., 1968. Dimensional grain orientation of Ordovician turbidite greywackes. *J. Sediment. Petrol.,* 38:164–174.

Parkash, B., and Middleton, G.V., 1970. Downcurrent textural changes in Ordovician turbidite greywackes. *Sedimentology,* 14(3–4):259–293. **doi:10.1111/j.1365-3091.1970.tb00195.x**

Pe-Piper, G., and Piper, D.J.W., 2004. The effects of strike-slip motion along the Cobequid–Chedabucto–southwest Grand Banks fault system on the Cretaceous–Tertiary evolution of Atlantic Canada. *Can. J. Earth Sci.,* 41(7):799–808. **doi:10.1139/e04-022**

Pickering, K., Hiscott, R., and Hein, R., 1989. *Deep-Marine Environments: Clastic Sedimentation and Tectonics:* London (Unwin-Hyman).

Potter, P.E., and Pettijohn, F.J., 1963. *Paleocurrents and Basin Analysis:* Berlin (Springer-Verlag).

Rees, A.I., 1965. The use of anisotropy of magnetic susceptibility in the estimation of sedimentary fabric. *Sedimentology,* 4(4):257–271. **doi:10.1111/j.1365-3091.1965.tb01550.x**

Sanford, B.V., Grant, A.C., Wade, J.A., and Barss, M.S., 1979. *Geology of Eastern Canada and Adjacent Areas*. Map.—Geol. Surv. Can., 1401A.

Schenk, P.E., 1995. Meguma zone. *In* Williams, H. (Ed.), *The Geology of North America* (Vol. 6): *Geology of the Appalachian–Caledonian Orogen in Canada and Greenland:* Boulder (Geol. Soc. Am.), 261–277.

Shillington, D.J., Holbrook, W.S., Van Avendonk, H.J.A., Tucholke, B.E., Hopper, J.R., Louden, K.E., Larsen, H.C., and Nunes, G.T., 2006. Evidence for asymmetric nonvolcanic rifting and slow incipient oceanic accretion from seismic reflection data on the Newfoundland margin. *J. Geophys. Res.,* 111(B9):B09402. **doi:10.1029/2005JB003981**

Shipboard Scientific Party, 2004a. Leg 210 summary. *In* Tucholke, B.E., Sibuet, J.-C., Klaus, A., et al., *Proc. ODP, Init. Repts.,* 210: College Station, TX (Ocean Drilling Program), 1–78. **doi:10.2973/odp.proc.ir.210.101.2004**

Shipboard Scientific Party, 2004b. Explanatory notes. *In* Tucholke, B.E., Sibuet, J.-C., Klaus, A., et al., *Proc. ODP, Init. Repts.,* 210: College Station, TX (Ocean Drilling Program), 1–69. **doi:10.2973/odp.proc.ir.210.102.2004**

Spotts, J.H., 1964. Grain orientation and imbrication of Miocene turbidity current sandstones, California. *J. Sediment. Petrol.,* 34:229–253.

Srivastava, S.P., and Verhoef, J., 1992. Evolution of Mesozoic sedimentary basins around the North Central Atlantic: a preliminary plate kinematic solution. *In* Par-

nell, J. (Ed.), *Basins of the Atlantic Seaboard: Petroleum Geology, Sedimentology and Basin Evolution*. Spec. Publ.—Geol. Soc. London, 62:397–420.

Taira, A., 1976. Grain orientation and depositional processes—fabric analyses of modern and laboratory flume deposits [Ph.D. thesis]. Univ. Texas, Dallas.

Williams, H., O'Brien, S.J., King, A.F., and Anderson, M.M., 1995. Avalon Zone—Newfoundland. *In* Keen, M.J., and Williams, G.L. (Eds.), *The Geology of North America* (Vol. 2): *Geology of the Continental Margin of Eastern Canada:* Boulder (Geol. Soc. Am.), 226–237.

Ziegler, P.A. (Ed.), 1988. Evolution of the Arctic-North Atlantic and the western Tethys. *AAPG Mem.,* 43.

Zuffa, G.G., 1985. Optical analyses of arenites: influence of methodology on compositional results. *In* Zuffa, G.G. (Ed.), *Provenance of Arenites*. NATO ASI Ser., Ser. C, 148:165–189.

Zuffa, G.G., Normark, W.R., Serra, F., and Brunner, C.A., 2000. Turbidite megabeds in an oceanic rift valley recording Jökulhlaups of late Pleistocene glacial lakes of the western United States. *J. Geol.,* 108(3):253–274. **doi:10.1086/314404**

Figure F1. Location of ODP Site 1276 east of the Grand Banks of Newfoundland. Contours in meters.

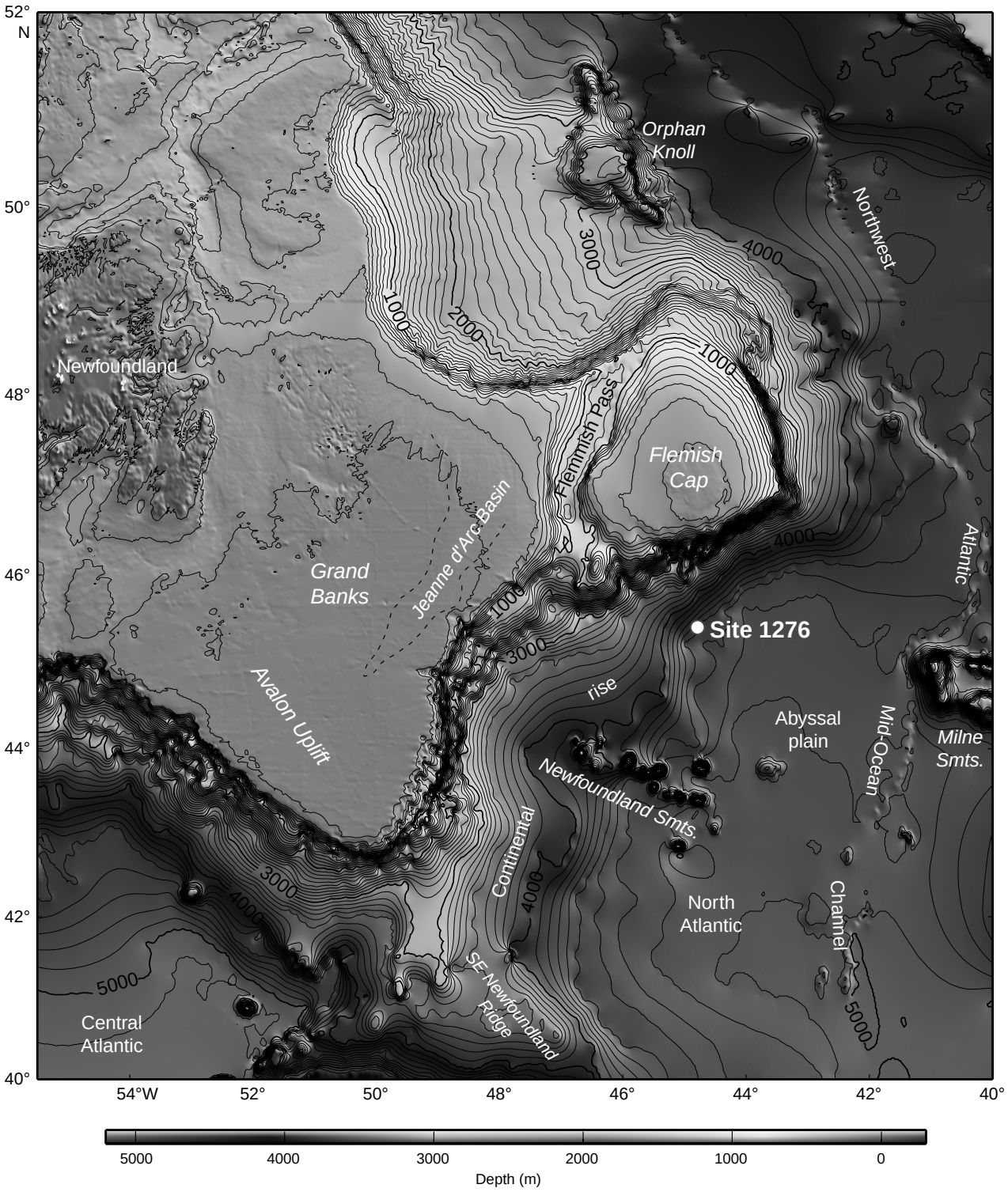

Figure F2. Lithologic column for Hole 1276A (left: Shipboard Scientific Party, 2004a) correlated to the time-equivalent stratigraphy in the Jeanne d'Arc Basin of the Grand Banks (right: Deptuck et al., 2003; Ainsworth et al., 2005). Dark blue grain-size labels denote grades of sand. SM = South Mara, FH = Fox Harbour, OB = Otter Bay, Mbr. = member.

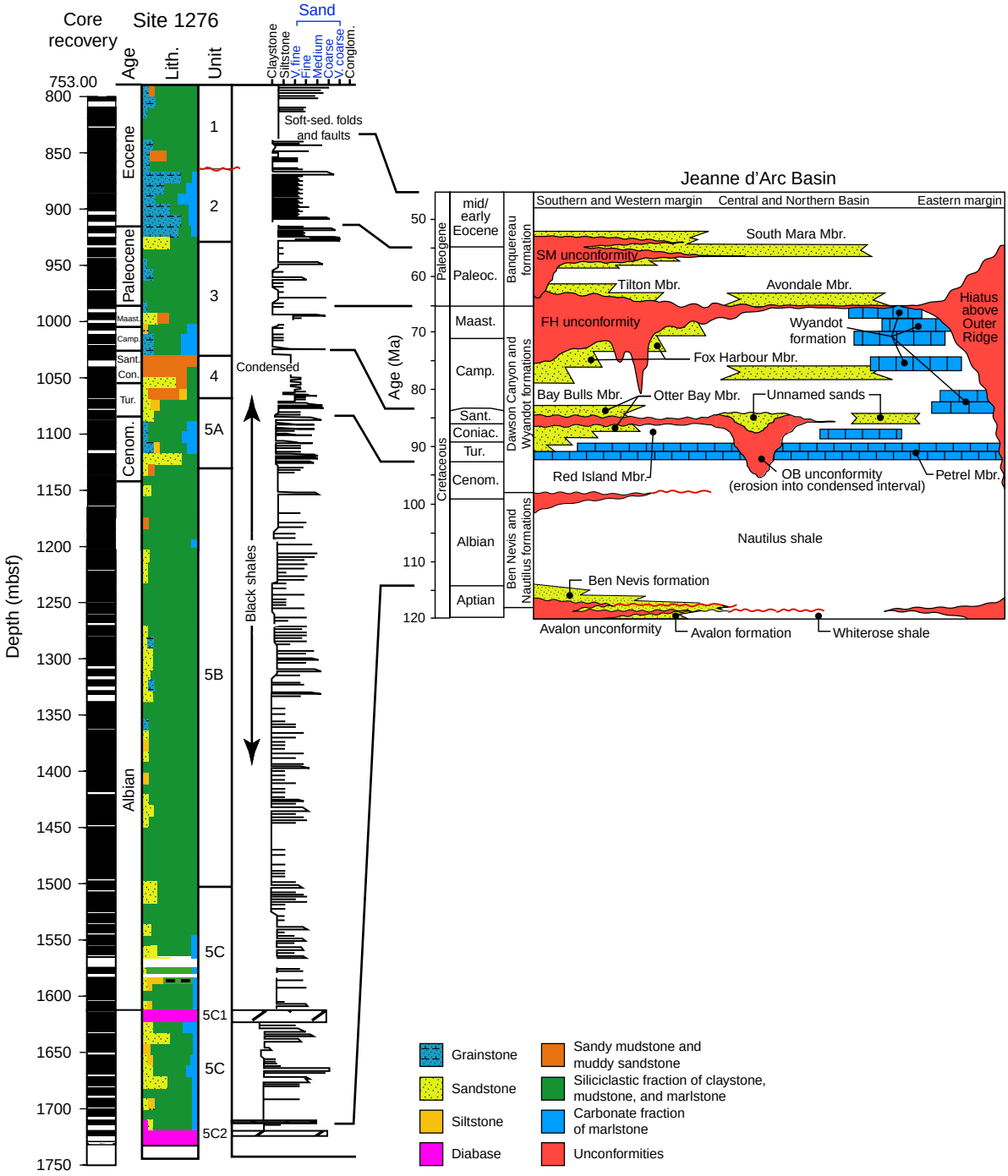

Figure F3. Graphic section of Cores 210-1276A-89R to 93R showing very thick bedded mud-dominated turbidites (in white) toward the base of the Albian succession in Hole 1276A. The fine-grained bed tops of these organized gravity flow deposits contain pseudonodules and ductile deformation structures; basal divisions are planar laminated and locally cross-laminated. Interbedded shale is pale gray. Disorganized sandy to pebbly debris flow deposits (DF) are dark gray.

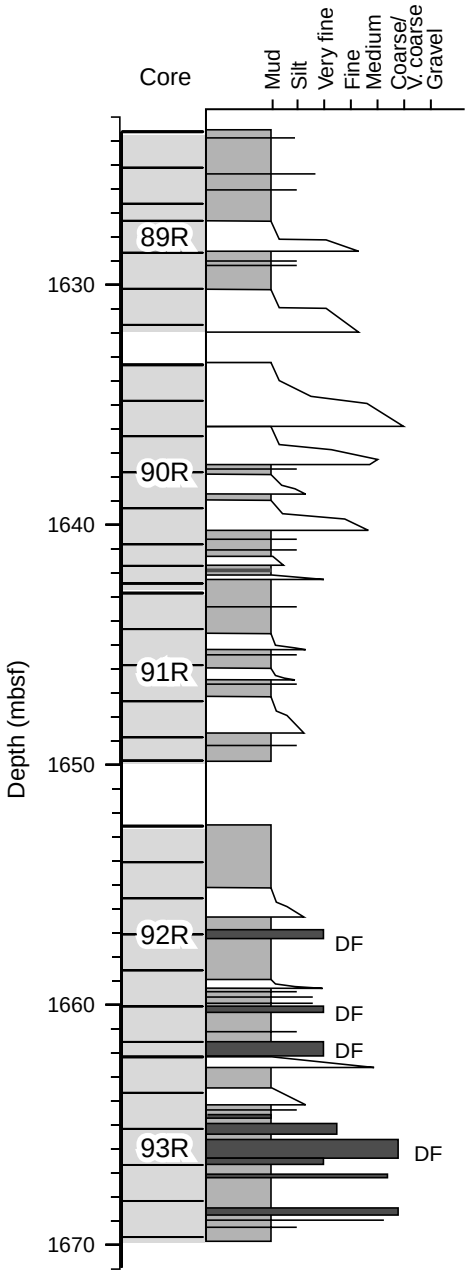

Figure F4. Reconstructions of the Cretaceous North Atlantic region. **A.** Albian (~110 Ma; Ziegler, 1988; Andeweg, 2002), with patterns explained in the key. **B.** Aptian at M0 Chron (~118 Ma; Srivastava and Verhoef, 1992), with ODP sites labeled and dark shading of modern land area. Pale shading in B indicates Jurassic–Cretaceous basins. CB = Cantabrian Basin, CSB = Celtic Sea Basin, FC = Flemish Cap, GLB = Galicia Bank, HB = Horseshoe Basin, IAP = Iberia Abyssal Plain, IGB = Inner Galicia Basin, JB = Jeanne d'Arc Basin, LB = Lusitanian Basin, OB = Orphan Basin, PB = Porcupine Basin, SENR = Southeast Newfoundland Ridge, TAP = Tagus Abyssal Plain, WAB = Western Approaches Basin. ODP holes on the Iberian margin are indicated by black dots and are labeled with site numbers. Site 1276 (open circle) is also shown.

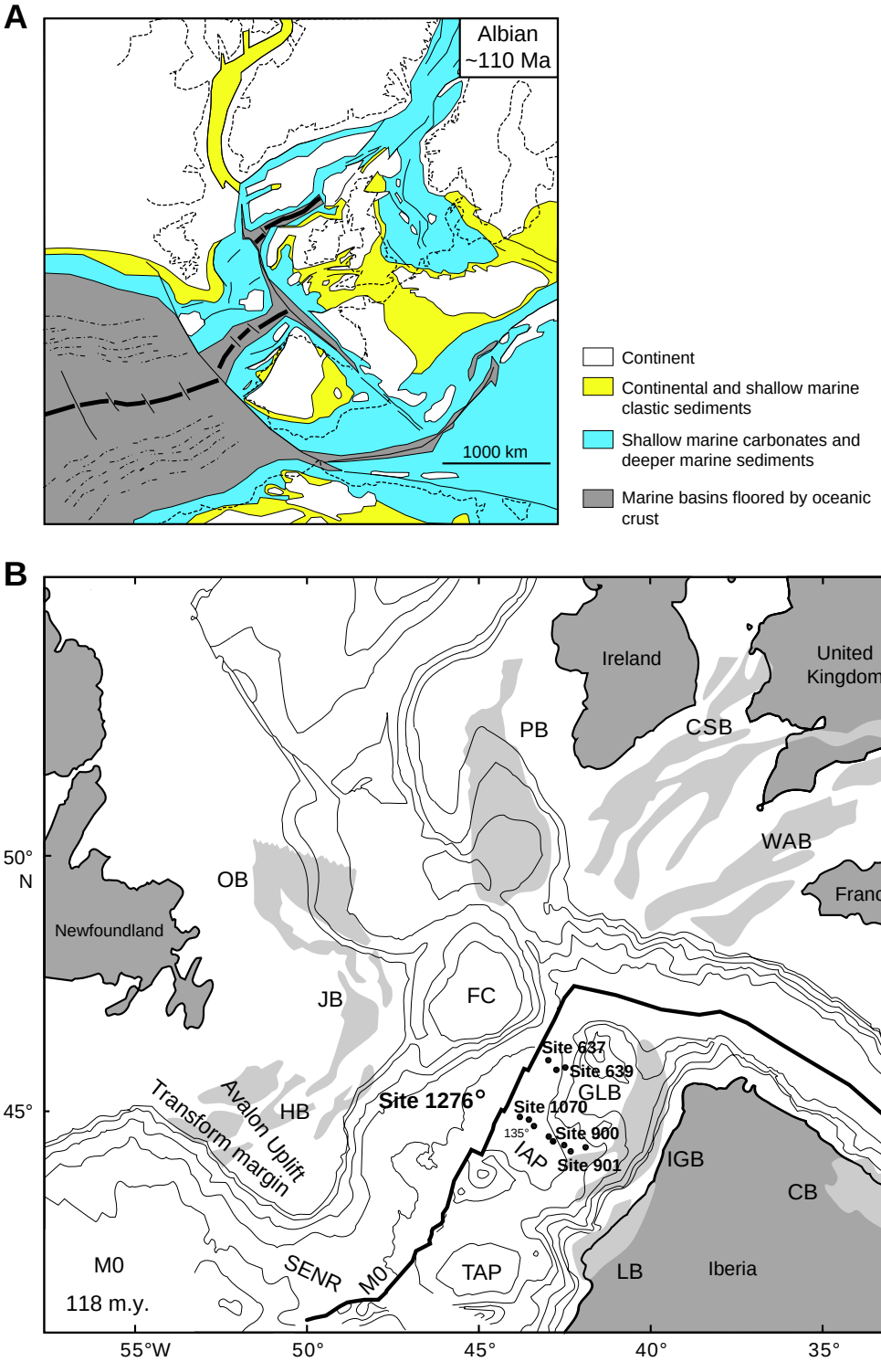

Figure F5. Depth-converted seismic reflection profiles through Site 1276, from Shillington et al. (2006). Dip Line 2 and strike Line 303 cross at Site 1276. Compass bearings of the ends of the lines are provided. Vertical exaggeration (VE) is 3×. The Albian section is indicated by a double-headed green arrow in both profiles. Apparent dips of reflections are marked with red line segments, with dip angles corrected for VE. Duplicate uninterpreted segments of the central parts of each profile are provided below for comparison. True dips and dip directions are listed in Table T1, p. 24.

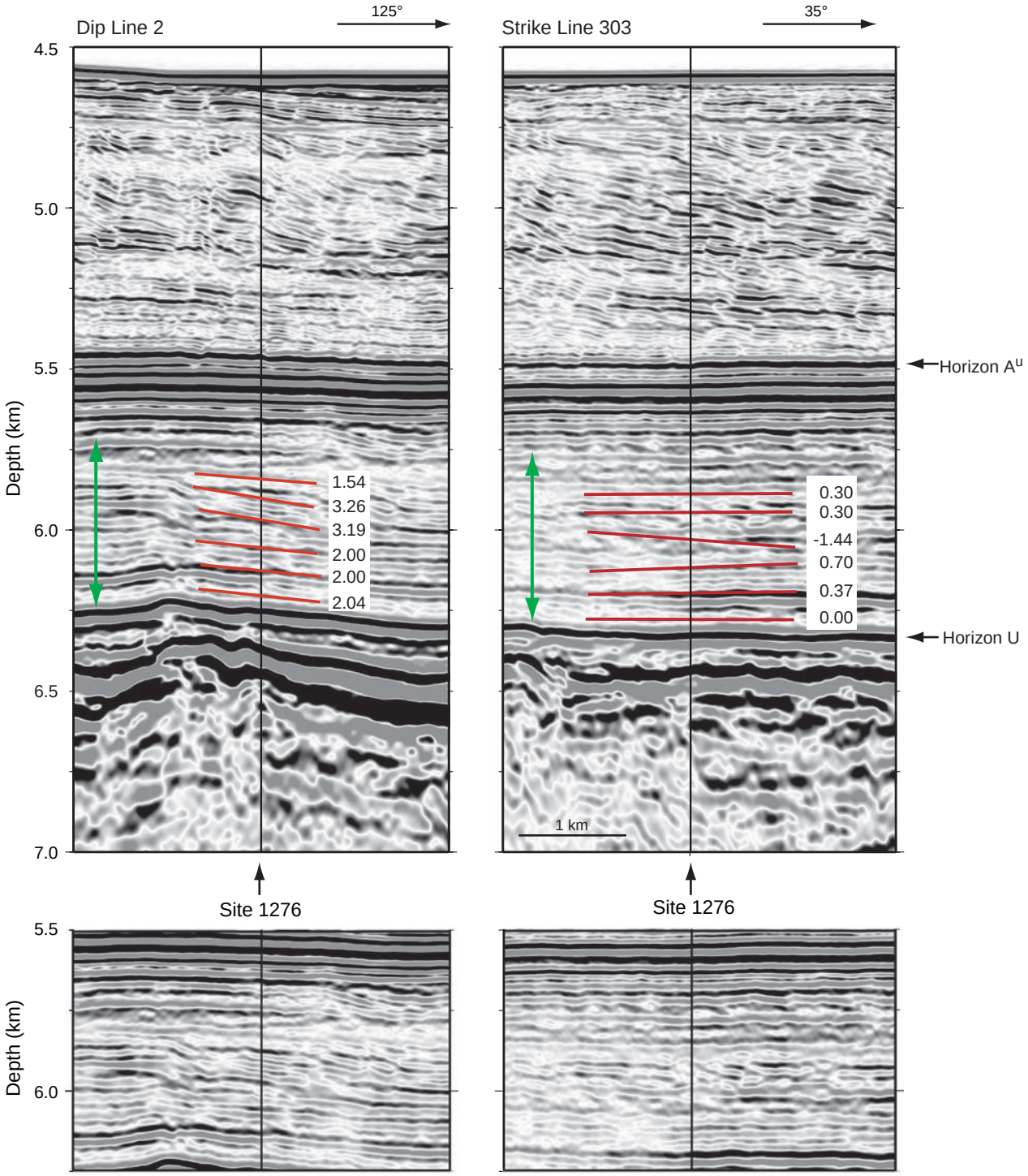

Figure F6. Average core-by-core maximum dip, plotted against the depths of core tops. The number of individual dip determination contributing to each point is indicated by color coding. The dips were measured using XVIEW software. The line of best fit was generated by Microsoft Excel. Scatter about this line decreases as the number of dip determinations per core increases.

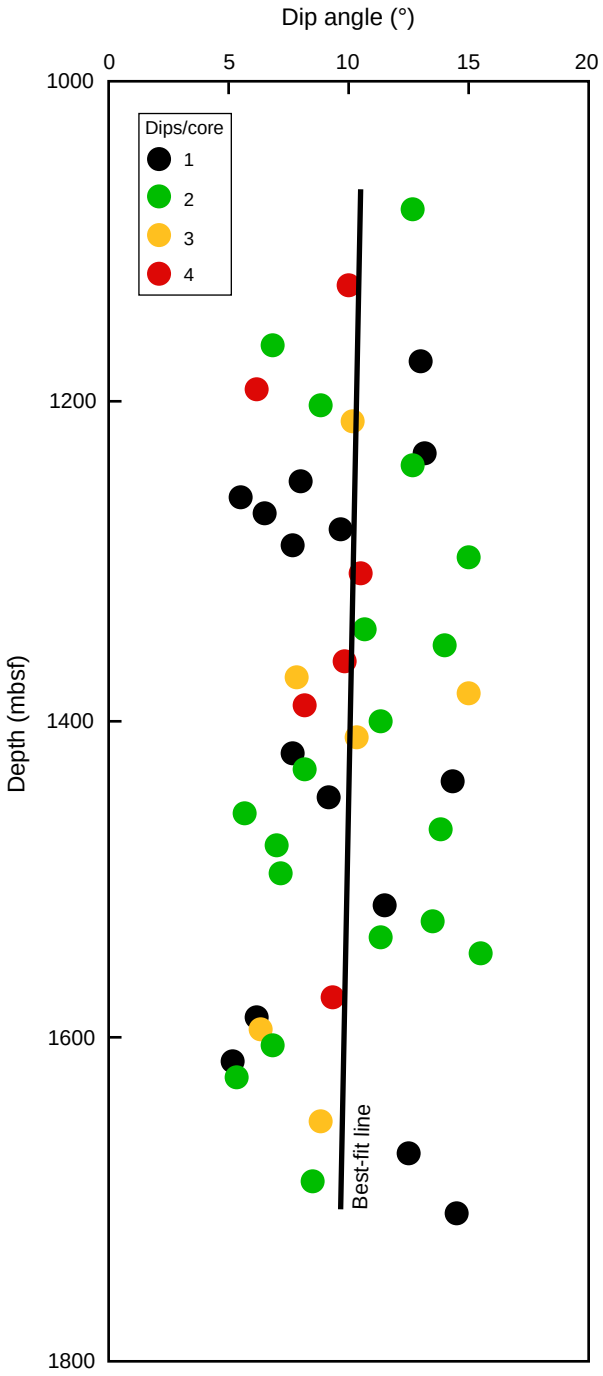

Figure F7. Equal-area rose diagrams, with 10° bin size, summarizing the bed-parallel grain fabric of 11 samples with a χ^2 significance level ≤0.10. Data for all 16 samples are in Table **T3,** p. 26. North is up. Paleoflow directions (red arrows) are based on imbrication results in Figure **F8,** p. 22, and Table **T4,** p. 27.

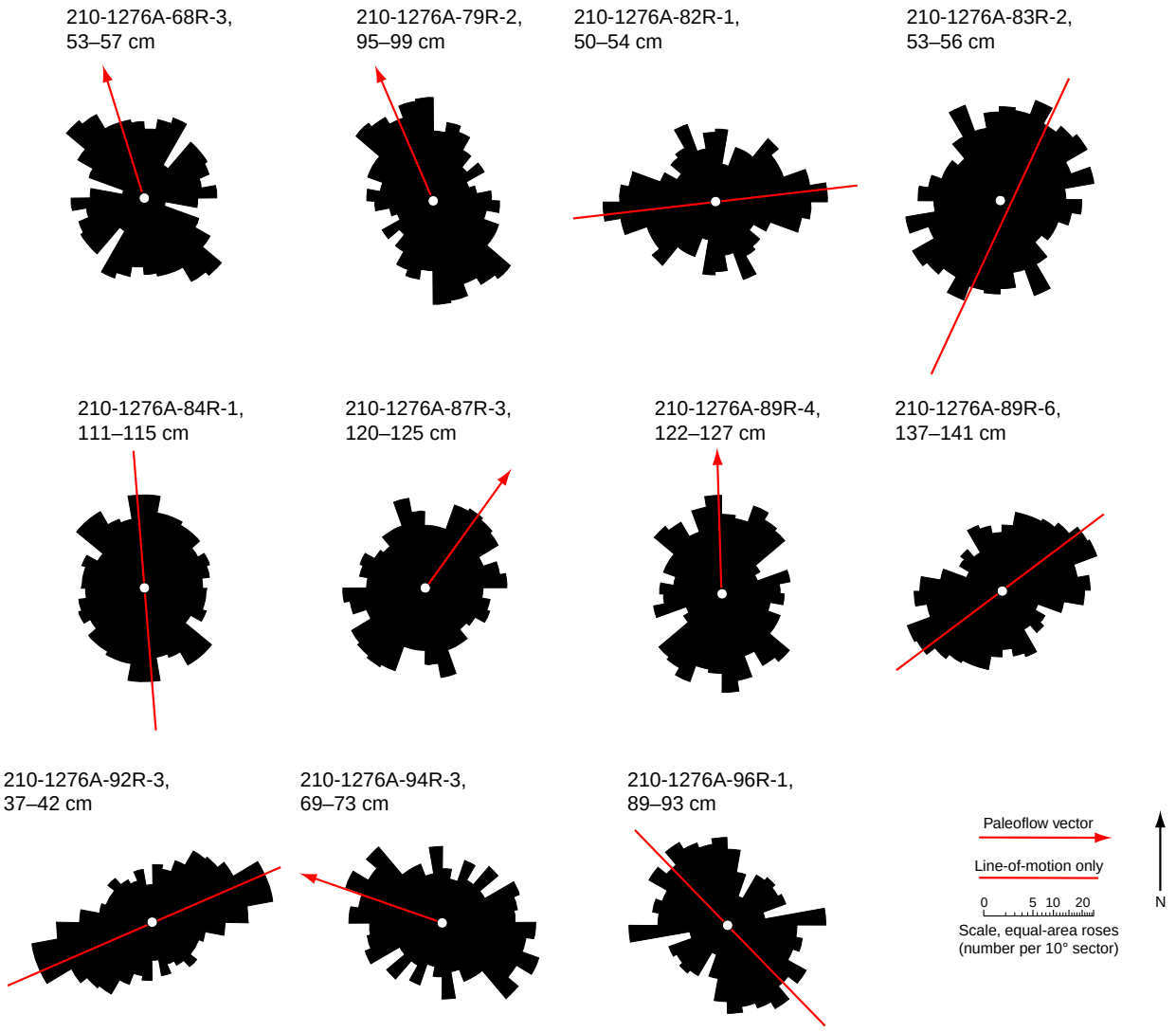

Figure F8. Equal-area rose diagrams, with 10° bin size, summarizing the bed-perpendicular grain fabric of the 11 samples in Figure F7, p. 21. All thin sections were cut parallel with the bed-parallel vector mean. All samples have a χ^2 significance level ≤0.005. The bedding is horizontal. Paleoflow directions are only given, with an arrow, for the five samples with imbrication ≥8°. Data for each sample are in Table T4, p. 27.

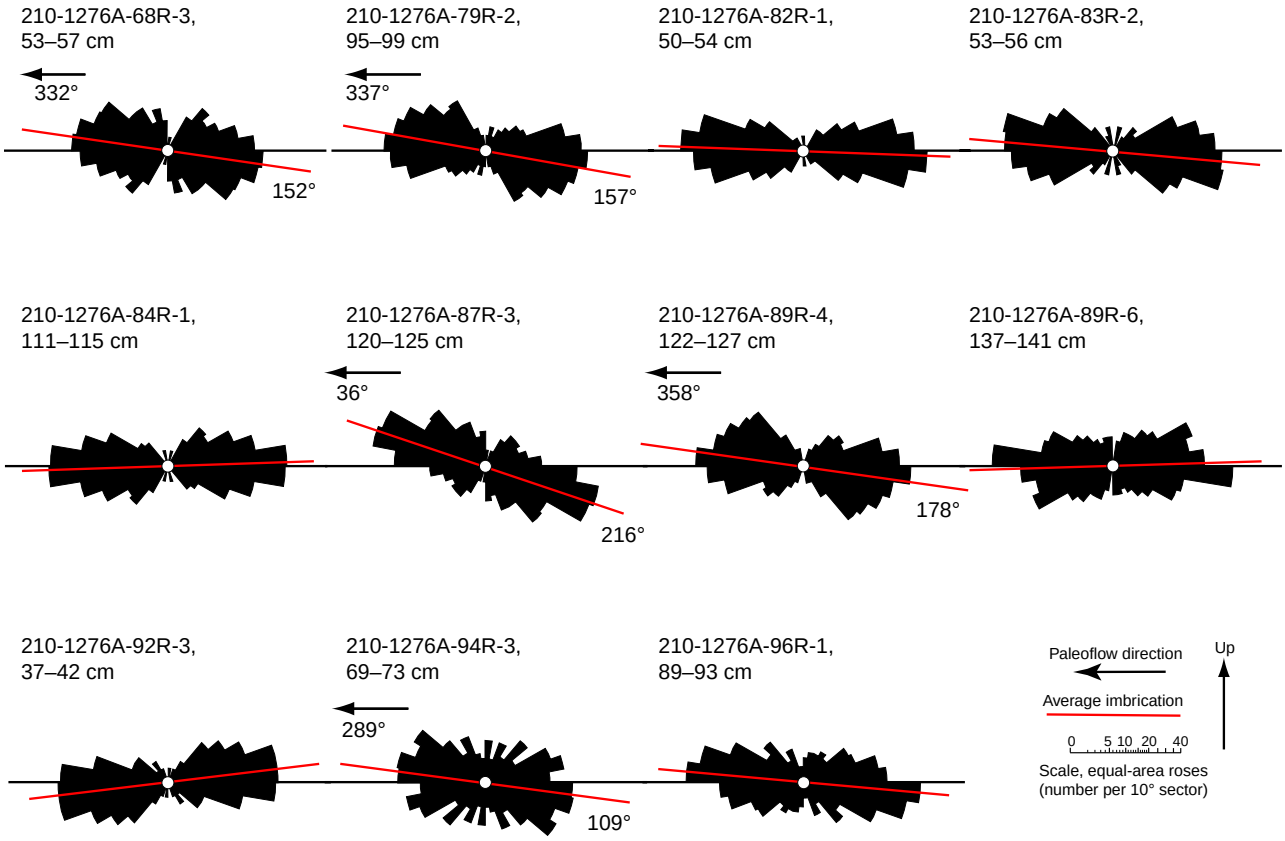

Figure F9. Unit vector plots of 11 ripple foreset dips (gray arrows) and the vector means for 11 grain-fabric determinations (black lines). In five cases where imbrication results defined a unique flow direction, the black lines have arrow heads indicating the paleoflow direction. In the other cases, the vector means are plotted to be as consistent as possible with the known flow directions, although the data do permit a 180° rotation of these vectors. Two cases are presented. **A.** The reference line is oriented downdip toward 130°. **B.** The reference line is rotated 30° clockwise to an azimuth of 160°. The M0 map is a cropped version of Figure F4, p. 18. FC = Flemish Cap, GLB = Galicia Bank, HB = Horseshoe Basin, IAP = Iberia Abyssal Plain, JB = Jeanne d'Arc Basin, LB = Lusitanian Basin, SENR = Southeast Newfoundland Ridge, TAP = Tagus Abyssal Plain, WB = Whale Basin, ? = least likely dispersal pathway (originating in the vicinity of several rift basins on the Grand Banks).

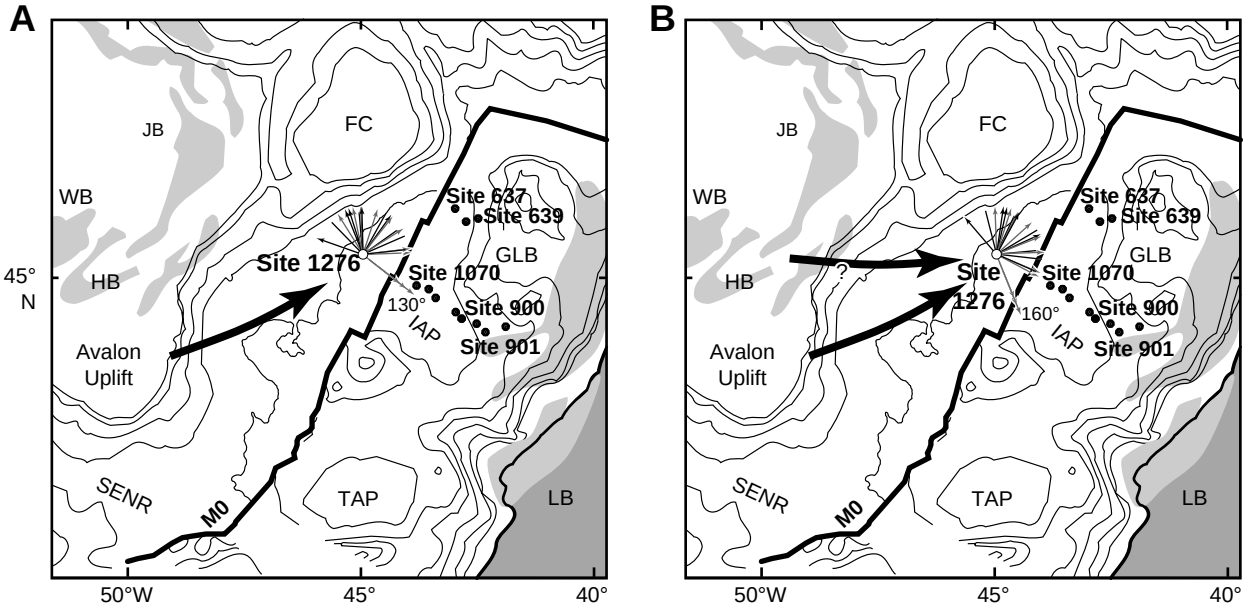

Table T1. Apparent dips and calculated true dips of six prominent reflections marked on seismic-reflection profiles of Figure **F5,** p. 19.

Reflection	Angle in profile* (°)	Tan angle	Tan/3	Corrected apparent dip (°)	From *Stereonet*† (°)		
					Strike	Dip line	True dip angle
	Line 2						
1	4.60	0.080	0.027	1.54	46.0	136.0	1.57
2	9.70	0.171	0.057	3.26	40.3	130.3	3.27
3	9.50	0.167	0.056	3.19	10.8	100.8	3.50
4	6.00	0.105	0.035	2.01	54.2	144.2	2.13
5	6.00	0.105	0.035	2.01	45.4	135.4	2.04
6	6.10	0.107	0.036	2.04	35.0	125.0	2.04
	Line 303						
1	0.90	0.016	0.005	0.30			
2	0.90	0.016	0.005	0.30			
3	–4.30	–0.075	–0.025	–1.44			
4	2.10	0.037	0.012	0.70			
5	1.10	0.019	0.006	0.37			
6	0.00	0.000	0.000	0.00			
	Average dip direction and amount:					128.6	2.43

Notes: * = with vertical exaggeration. † = columns present values of true strike and dip obtained from software of the same name (see **"Data and Methods,"** p. 4).

Table T2. Ripple migration directions recorded in core pieces and referenced to the maximum dip direction in the same interval.

Core, section, interval (cm)	Depth (mbsf)	Degrees clockwise from dip direction*	Paleoflow (°) for 130° reference
210-1276A-			
38R-5, 120	1152.60	(090)	040
44R-2, 107	1205.80	(130)	000
44R-6, 10	1210.92	000	130
45R-2, 92	1215.25	(070)	060
51R-4, 90	1276.10	000	130
55R-1, 35	1309.55	(040)	090
67R-1, 130	1422.20	000	130
77R-4, 50	1521.90	(110)	020
83R-1, 40	1574.90	(150)	340
83R-3, 6	1577.56	(140)	350
92R-3, 65	1656.16	(045)	085
		Average paleoflow:	060

Note: * = values in parentheses are counterclockwise from dip direction.

Table T3. Summary statistics for grain fabric measured in 16 thin sections cut parallel with planar laminae of T_b divisions of turbidites.

Core, section, interval (cm)	Depth (mbsf)	υ (°)	L (%)	SL less than this value
210-1276A-				
55R-1, 73–77	1309.93	(125)	11.23	0.200
67R-1, 70–74	1421.60	(029)	6.34	1.000
67R-5, 120–125	1428.10	(171)	3.96	1.000
68R-3, 53–57	1434.03	162	16.92	0.005
79R-2, 95–99	1538.65	157	34.06	0.005
82R-1, 50–54	1565.50	083	22.88	0.005
83R-2, 53–56	1576.53	029	18.24	0.005
84R-1, 111–115	1585.31	175	16.20	0.010
85R-4, 103–107	1592.48	(129)	7.82	0.200
87R-3, 120–125	1608.74	036	13.84	0.025
89R-4, 122–127	1628.53	178	22.58	0.005
89R-6, 137–141	1631.51	053	28.17	0.005
90R-5, 68–71	1641.45	(071)	6.23	1.000
92R-3, 37–42	1655.87	066	43.17	0.005
94R-3, 69–73	1675.34	109	25.66	0.005
96R-1, 89–93	1691.79	136	22.74	0.005

Notes: υ = vector mean. L = vector magnitude. SL = significance level. Vector means are based on a 130° reference direction and are presented as angles in the range 0°–179°. Nonsignificant vector means are in parentheses.

Table T4. Summary statistics for grain fabric measured in 11 sections cut perpendicular to planar laminae of T_b divisions of turbidites.

Core, section, interval (cm)	Depth (mbsf)	υ (°)	L (%)	SL less than this value	Decision on flow direction (°)
210-1276A-					
68R-3, 53–57	1434.03	172	55.24	0.005	332
79R-2, 95–99	1538.65	010	66.06	0.005	337
82R-1, 50–54	1565.50	(002)	81.89	0.005	083 or 263
83R-2, 53–56	1576.53	(005)	76.46	0.005	029 or 209
84R-1, 111–115	1585.31	(178)	77.80	0.005	175 or 355
87R-3, 120–125	1608.74	019	63.88	0.005	036
89R-4, 122–127	1628.53	008	68.90	0.005	358
89R-6, 137–141	1631.51	(178)	61.67	0.005	053 or 233
92R-3, 37–42	1655.87	(173)	76.78	0.005	066 or 246
94R-3, 69–73	1675.34	008	44.92	0.005	289
96R-1, 89–93	1691.79	(005)	63.88	0.005	136 or 316

Notes: υ = vector mean. L = vector magnitude. SL = significance level. Vector means are based on a 130° reference direction and are presented as angles in the range 0°–179°. Nonsignificant vector means (<8° or >172°) are in parentheses. Flow directions are relative to true north, based on a 130° reference direction.